Field dependence of the residual-resistivity anisotropy in sodium and potassium

M. Huberman
Department of Physics, Michigan Technological University, Houghton, Michigan 49931

A. W. Overhauser
Department of Physics, Purdue University, West Lafayette, Indiana 47907

(Received 15 August 1984)

Recent measurements of the low-field, induced torque in sodium and potassium by Elliott and Datars show that the resistivity anisotropy increases with increasing magnetic field. The zero-field resistivity anisotropy, unexpected for cubic symmetry, is explained by the charge-density-wave (CDW) structure. Due to the wave-function mixing caused by the CDW potential, the momentum transfer (by isotropic impurities) is much larger for electrons near the CDW energy gap. This is modeled by an anisotropic relaxation time in $\vec{k}$ space. The Boltzmann transport equation in a magnetic field can then be solved exactly. The computed resistivity anisotropy is higher for $\omega_c\tau > 1$ compared with its zero-field value. The effect of the magnetic field is to "stir" the electron distribution $f(\vec{k})$; this feeds electrons into the region of rapid relaxation and thereby increases the resistivity anisotropy.

I. INTRODUCTION

The induced torque of sodium and potassium spheres has different character at low (0—5 kG), intermediate (5—40 kG), and high (>40 kG) magnetic fields, each stemming from a charge-density-wave (CDW) structure.[1] At low fields, the torque as a function of magnet rotation angle has a twofold, sinusoidal pattern,[2,3] caused by a residual-resistivity anisotropy.[4] At intermediate fields, it has a smooth, four-peak pattern,[2,3] caused by an anisotropic Hall coefficient.[5] At high fields, it exhibits many sharp peaks,[6,7] caused by open orbits.[8]

Recently Elliott and Datars discovered that the magnitude of the twofold, torque anisotropy increases with increasing magnetic field.[9,10] An example of their data for potassium is shown in Fig. 1. The deviation of the torque ratio from unity increases by an order of magnitude. Bishop and Overhauser have shown that, if a field-independent resistivity anisotropy is assumed, the torque anisotropy decreases with increasing field.[4] The correct approach, however, is to derive the magnetoresistivity by solving the Boltzmann transport equation. When this is done, the resistivity anisotropy is found to increase with field, explaining the rise of the torque anisotropy.

The zero-field resistivity anisotropy is caused by the CDW potential $V = G\cos(\vec{Q}\cdot\vec{r})$.[4] The Fermi surface in the repeated-zone scheme is shown in Fig. 2. Because Q is approximately equal to the Fermi-surface diameter, electron states at the Fermi surface near the conical points $\pm\vec{Q}/2$ are strongly perturbed, the plane waves $\vec{k}$ and $\vec{k}\pm\vec{Q}$ being mixed. In normal electron-impurity scattering, the wave-vector transfer $\vec{q}$ is small, since the impurity potential has small $-q$ Fourier components. Due to the wave-function mixing, however, electrons near the CDW energy gap can also suffer a much larger wave-vector transfer $\vec{q}\pm\vec{Q}$ (CDW—umklapp scattering). Since large-angle scattering contributes more to the resistivity than small-angle scattering, the residual resistivity is higher parallel to $\vec{Q}$ than perpendicular to $\vec{Q}$.

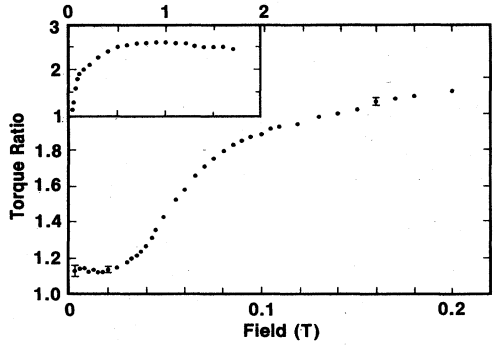

FIG. 1. The ratio of the twofold torque maximum and minimum for a potassium sphere (Elliott and Datars, Ref. 10).

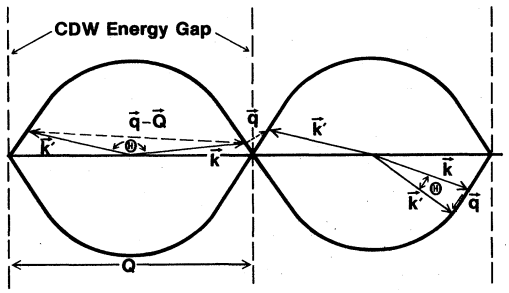

FIG. 2. Electron-impurity normal scattering ($\Delta\vec{k}=\vec{q}$) and CDW—umklapp scattering ($\Delta\vec{k}=\vec{q}-\vec{Q}$). $\vec{Q}$ is the CDW wave vector.

In order to solve the Boltzmann transport equation in a magnetic field, we model the impurity scattering by an anisotropic relaxation time in $\vec{k}$ space. The large momentum transfer near the conical points $\pm\vec{Q}/2$ is mimicked by a rapid relaxation rate. In zero magnetic field, the steady-state distribution $f(\vec{k})$ is nonspherical, being displaced less (from the equilibrium distribution) where the relaxation time is short. The effect of a magnetic field is to "stir" the distribution function, feeding electrons into the region of rapid relaxation. This increases the resistivity anisotropy and thereby the torque anisotropy.

II. ANISOTROPIC RELAXATION TIME

We approximate the Fermi surface by a sphere, neglecting the distortion near the energy-gap planes. The relaxation time of an electron at the Fermi energy has uniaxial symmetry. We model it by

$$\tau(\theta)=\begin{cases}\tau\,, & |\cos\theta|<\cos\eta\\ \tau'\,, & |\cos\theta|>\cos\eta\end{cases} \tag{1}$$

where θ is the angle between the electron wave vector $\vec{k}$ and the CDW wave vector $\vec{Q}$ (Fig. 3). Since the resistivity is higher parallel to $\vec{Q}$, τ' is shorter than τ. The angle η defines the region of umklapp scattering. A microscopic argument, presented in the Appendix, indicates $\eta\approx 25°$ for sodium and potassium. The fraction of electrons on the Fermi surface experiencing rapid relaxation is then about 10%.

Semiclassical transport theorems[11] predict for a simply connected Fermi surface that the magnetoresistance saturates and the Hall coefficient is isotropic, when $\omega_c\tau>1$. Since the assumed Fermi surface is simply connected, the model omits the nonsaturating magnetoresistance and (high-field) Hall-coefficient anisotropy.

This model has one adjustable parameter, the relaxation-time ratio τ'/τ. The magnitude of the torque-anisotropy increase is approximately explained by choosing $\tau'/\tau\approx 0.05$. Such a large anisotropy of the relaxation time $\tau(\theta)$ is not inconsistent with the small anisotropy (about 10%) of electron-impurity scattering deduced from de Haas–van Alphen effect studies.[12] $\tau(\theta)$ is a momentum-relaxation lifetime, weighting large-angle scattering more heavily than small-angle scattering, whereas the ordinary lifetime determined by the de Haas–van Alphen effect weights all collisions equally.

The model (1) focuses on the essential feature causing the torque-anisotropy rise, namely, anisotropic scattering. It has the significant advantage of being tractable (at any magnetic-field strength). Its drawback, of course, is that it is not derived microscopically.

III. ZERO-FIELD RESISTANCE

The Boltzmann equation for the steady-state electron distribution $f(\vec{k})$ is

$$-\frac{e}{\hbar}\vec{E}\cdot\vec{\nabla}_{\vec{k}}f-\frac{e}{\hbar c}(\vec{v}\times\vec{B})\cdot\vec{\nabla}_{\vec{k}}f=-\frac{f-f_0}{\tau(\theta)}\,. \tag{2}$$

Letting $g\equiv f-f_0$ be the deviation from equilibrium yields

$$-e\vec{E}\cdot\vec{v}\frac{df_0}{d\epsilon}-\frac{e}{\hbar c}(\vec{v}\times\vec{B})\cdot\vec{\nabla}_{\vec{k}}g=-\frac{g}{\tau(\theta)} \tag{3}$$

to first order in $\vec{E}$. In zero magnetic field, the immediate solution is

$$g=\tau(\theta)e\vec{E}\cdot\vec{v}\frac{df_0}{d\epsilon}\,, \tag{4}$$

the electron distribution

$$f=f_0+g\cong f_0(\vec{k}+[\tau(\theta)e/\hbar]\vec{E}) \tag{5}$$

being illustrated (for $\vec{E}$ parallel to $\vec{Q}$) in Fig. 4.

Evaluating the current density yields the electrical conductivity. For a degenerate equilibrium distribution, the resistivities parallel and perpendicular to $\vec{Q}$ are

$$\rho_{\parallel}=\frac{m}{ne^2\langle\tau(\theta)\rangle_{\parallel}}\,,\quad \rho_{\perp}=\frac{m}{ne^2\langle\tau(\theta)\rangle_{\perp}}\,, \tag{6}$$

the weighted angular averages over the Fermi surface being defined by

$$\langle\tau(\theta)\rangle_{\parallel}\equiv\frac{3}{4\pi}\int d\Omega\,\cos^2\theta\,\tau(\theta)\,,$$
$$\langle\tau(\theta)\rangle_{\perp}\equiv\frac{3}{8\pi}\int d\Omega\,\sin^2\theta\,\tau(\theta)\,. \tag{7}$$

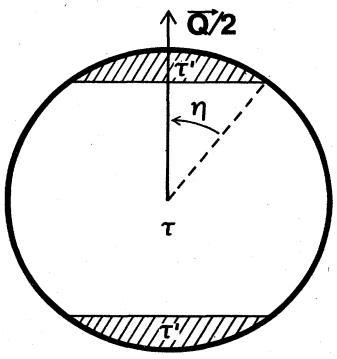

FIG. 3. Anisotropic relaxation-time on the Fermi surface. $\vec{Q}$ is the CDW wave vector.

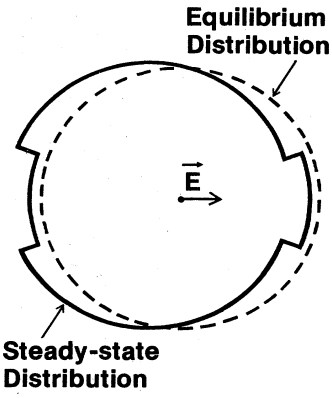

FIG. 4. Zero-field steady-state distribution $f(\vec{k})$ for $\vec{E}\|\vec{Q}$.

Substituting (1) for $\tau(\theta)$, we find

$$\rho_{\parallel}=\rho_0\left[1-\left[1-\frac{\tau'}{\tau}\right](1-\cos^3\eta)\right]^{-1},$$
$$\rho_{\perp}=\rho_0\left[1-\left[1-\frac{\tau'}{\tau}\right](1-\tfrac{3}{2}\cos\eta+\tfrac{1}{2}\cos^3\eta)\right]^{-1}, \quad (8)$$

where $\rho_0\equiv m/(ne^2\tau)$. The resistivity anisotropy $\gamma\equiv\rho_{\parallel}/\rho_{\perp}$ is plotted in Fig. 5. For $\eta=25°$ and $\tau'/\tau=0.05$, $\rho_{\parallel}/\rho_0=1.32$, $\rho_{\perp}/\rho_0=1.01$, and $\gamma=1.30$.

It is instructive to evaluate the (zero-field) resistivity, assuming a rigidly shifted equilibrium distribution

$$f=f_0(\vec{k}-\vec{\delta}), \quad (9)$$

illustrated in Fig. 6. Evaluating the current density yields

$$\vec{J}=-ne\frac{\hbar\vec{\delta}}{m}. \quad (10)$$

The displacement $\vec{\delta}$, which is proportional to $\vec{E}$, is determined by balancing the momentum (per unit time) gained from the applied electric field and lost by collisions. Accordingly, the so-computed resistivities parallel and perpendicular to $\vec{Q}$ are

$$\rho'_{\parallel}=\frac{m}{ne^2}\left\langle\frac{1}{\tau(\theta)}\right\rangle_{\parallel}, \quad \rho'_{\perp}=\frac{m}{ne^2}\left\langle\frac{1}{\tau(\theta)}\right\rangle_{\perp}, \quad (11)$$

the angular averages having the same definitions as before.

By the variational principle,[13] the approximate resistivities (11) are higher than the exact resistivities (6). Substituting (1) for $\tau(\theta)$ yields

$$\rho'_{\parallel}=\rho_0\left[1+\left[\frac{\tau}{\tau'}-1\right](1-\cos^3\eta)\right],$$
$$\rho'_{\perp}=\rho_0\left[1+\left[\frac{\tau}{\tau'}-1\right](1-\tfrac{3}{2}\cos\eta+\tfrac{1}{2}\cos^3\eta)\right], \quad (12)$$

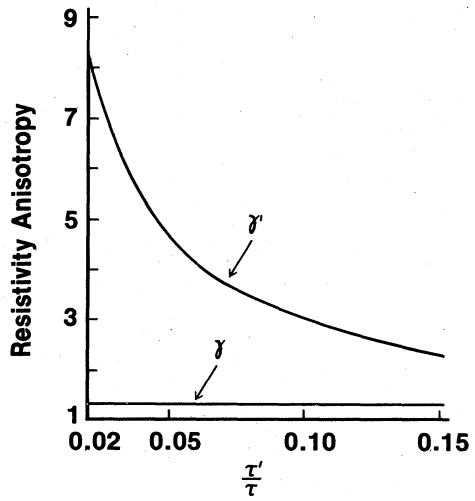

FIG. 5. Exact (γ) and approximate (γ') zero-field resistivity anisotropy. $\eta=25°$.

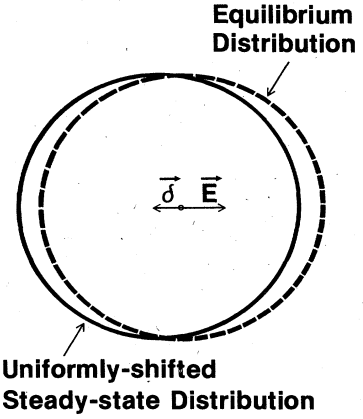

FIG. 6. Uniformly shifted, steady-state distribution $f(\vec{k})$. The displacement $\vec{\delta}$ depends on the direction of $\vec{E}$ relative to $\vec{Q}$.

where $\rho_0\equiv m/(ne^2\tau)$. The so-computed resistivity anisotropy $\gamma'\equiv\rho'_{\parallel}/\rho'_{\perp}$ is plotted in Fig. 5. For $\eta=25°$ and $\tau'/\tau=0.05$, $\rho'_{\parallel}/\rho_0=5.86$, $\rho'_{\perp}/\rho_0=1.24$, and $\gamma'=4.71$.

It is easy to understand why γ' is much larger than γ. For small angles η, the rapid relaxation affects primarily the parallel resistivities; the perpendicular resistivities ($\rho_{\perp}$ and $\rho'_{\perp}$) are approximately equal to ρ_0. In the exact distribution function for $\vec{E}\|\vec{Q}$, shown in Fig. 4, the deviation from equilibrium in the region of rapid relaxation is minimized. In the uniformly shifted distribution function, shown in Fig. 6, this deviation is much larger (for the same total current), many more electrons suffering rapid relaxation. Thus $\rho'_{\parallel}$ is much larger than $\rho_{\parallel}$.

In the next section, we calculate exactly the resistivity in a magnetic field. We shall show that the resistivity anisotropy γ', computed with a uniformly shifted distribution function, becomes exact when $\omega_c\tau>1$.

IV. MAGNETORESISTANCE

The magnetoresistance depends on the angle between $\vec{B}$ and $\vec{Q}$. We consider two orientations, $\vec{B}\|\vec{Q}$ and $\vec{B}\perp\vec{Q}$.

For these orientations, there are five resistivities, depicted in Fig. 7, and two Hall coefficients. The resistivity for

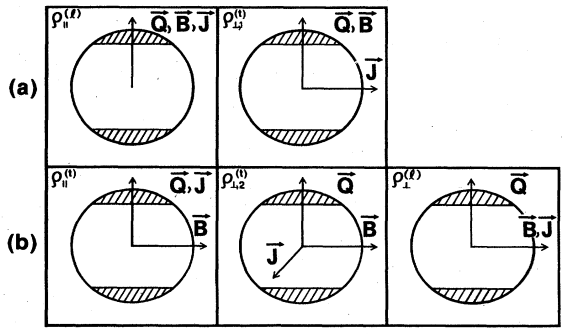

FIG. 7. Resistivities for (a) $\vec{B}\|\vec{Q}$ and (b) $\vec{B}\perp\vec{Q}$. $\vec{J}$ is the current.

a current $\vec{J}$ is either parallel or perpendicular, depending on whether $\vec{J}||\vec{Q}$ or $\vec{J}\perp\vec{Q}$, and longitudinal or transverse, depending on whether $\vec{J}||\vec{B}$ or $\vec{J}\perp\vec{B}$. There are two transverse, perpendicular resistivities, one with $\vec{Q}||\vec{B}$ and the other with $\vec{Q}\perp\vec{B}$. The two Hall coefficients are $R_{||}$ with $\vec{Q}||\vec{B}$ and $R_\perp$ with $\vec{Q}\perp\vec{B}$.

For $\vec{B}||\vec{Q}$, an electron's relaxation time is unchanged by its cyclotron motion. The Boltzmann equation (3) is easily solved by the ansatz

$$g=\tau(\theta)e\vec{A}\cdot\vec{v}\frac{df_0}{d\epsilon} \tag{13}$$

with $\vec{A}$ depending on $\cos\theta\equiv\hat{v}\cdot\hat{Q}$. For $\vec{B}=B\hat{z}$, the solution for $\vec{A}$ is

$$\begin{aligned} A_x&=\frac{E_x-\omega_c\tau E_y}{1+(\omega_c\tau)^2}\ ,\\ A_y&=\frac{E_y+\omega_c\tau E_x}{1+(\omega_c\tau)^2}\ ,\\ A_z&=E_z\ . \end{aligned} \tag{14}$$

$\omega_c=eB/mc$ is the cyclotron frequency; the θ dependence of τ is understood. Evaluating the current density yields the magnetoconductivity tensor

$$\sigma=\frac{ne^2}{m}\begin{vmatrix} \left\langle\frac{\tau}{1+(\omega_c\tau)^2}\right\rangle_\perp & -\left\langle\frac{\omega_c\tau^2}{1+(\omega_c\tau)^2}\right\rangle_\perp & 0\\ \left\langle\frac{\omega_c\tau^2}{1+(\omega_c\tau)^2}\right\rangle_\perp & \left\langle\frac{\tau}{1+(\omega_c\tau)^2}\right\rangle_\perp & 0\\ 0 & 0 & \langle\tau\rangle_{||} \end{vmatrix}, \tag{15}$$

the angular averages being defined as before.

The resistivity and Hall coefficient are obtained by inverting (15). Although the longitudinal resistivity

$$\rho_{||}^{(l)}=\frac{m}{ne^2\langle\tau\rangle_{||}} \tag{16}$$

is field independent, the transverse resistivity increases with field. Its saturation value is

$$\rho_\perp^{(t)}\to\frac{m}{ne^2}\left\langle\frac{1}{\tau}\right\rangle_\perp\ ,\quad \omega_c\tau>1\ , \tag{17}$$

equal to the resistivity $\rho_\perp'$, computed with a uniformly shifted distribution function.[14] The Hall coefficient decreases (in absolute value) with increasing field, being equal to the free-electron value $R_0=-1/(nec)$ when $\omega_c\tau>1$. The two resistivities ($\rho_{||}^{(l)}$ and $\rho_{\perp,1}^{(t)}$) and the Hall coefficient ($R_{||}$) are plotted in Figs. 8, 9, and 10 for $\tau(\theta)$ given by (1).

For $\vec{B}\perp\vec{Q}$, the magnetoconductivity can be derived by the effective-path method,[15] which is equivalent to solving the Boltzmann equation. The steady-state current density

$$\vec{J}=\frac{-2e}{\Omega}\sum_{\vec{k}}f(\vec{k})\vec{v}(\vec{k}) \tag{18}$$

is equal to the rate of change of the dipole moment per unit volume. Only electrons out of equilibrium need be considered, since the contribution from the equilibrium distribution vanishes. The applied electric field excites electrons out of equilibrium at the rate (to first order in $\vec{E}$)

$$\left[\frac{df}{dt}\right]_{\text{field}}=e\vec{E}\cdot\vec{v}(\vec{k})\frac{df_0}{d\epsilon}\ . \tag{19}$$

The average displacement (effective path) of an electron, created with wave vector $\vec{k}$, until it returns to equilibrium is

$$\vec{L}(\vec{k})=\int_0^\infty dt\,\vec{v}(\vec{k}(t))P(\vec{k},t)\ , \tag{20}$$

where the survival probability $P(\vec{k},t)$ is

$$P(\vec{k},t)=\exp\left[-\int_0^t\frac{dt'}{\tau(\vec{k}(t'))}\right]. \tag{21}$$

The current density $\vec{J}$ to first order in $\vec{E}$ is thus

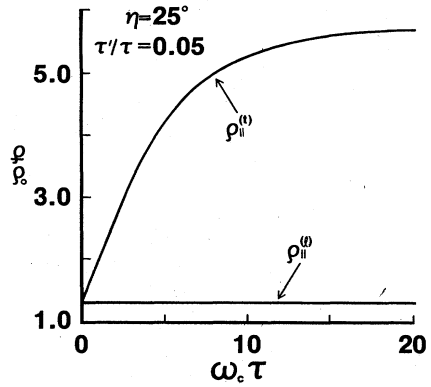

FIG. 8. Parallel resistivities vs magnetic-field strength. The saturation value of $\rho_{||}^{(t)}$ is $\rho_{||}'=5.86\rho_0$, where $\rho_0\equiv m/(ne^2\tau)$.

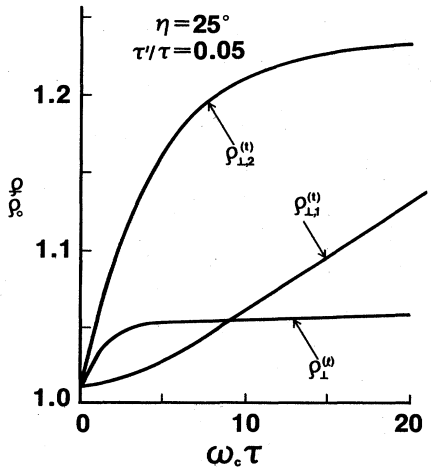

FIG. 9. Perpendicular resistivities vs magnetic-field strength. The saturation value of $\rho_{\perp,1}^{(t)}$ and $\rho_{\perp,2}^{(t)}$ is $\rho_\perp'=1.24\rho_0$, where $\rho_0\equiv m/(ne^2\tau)$. Note the different vertical scales in Figs. 8 and 9.

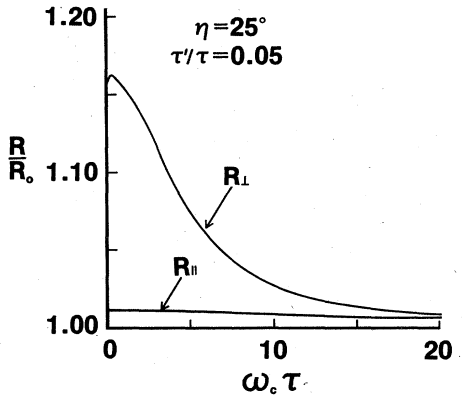

FIG. 10. Hall coefficients for $\vec{Q}||\vec{B}$ and $\vec{Q}\perp\vec{B}$. For $\omega_c\tau>1$, $R_{||}$ and $R_\perp$ are equal to $R_0\equiv -1/(nec)$.

$$\vec{J}=\frac{-2e}{\Omega}\sum_{\vec{k}} e\vec{E}\cdot\vec{v}(\vec{k})\frac{df_0}{d\epsilon}\int_0^\infty dt\,\vec{v}(\vec{k}(t))P(\vec{k},t)\ , \tag{22}$$

which is equivalent to the path-integral solution[16] of the Boltzmann equation.

In a magnetic field $\vec{B}=B\hat{z}$, the electron wave vector $\vec{k}$ rotates about $\vec{B}$ at the cyclotron frequency ω_c,

$$\vec{k}(t)=k\hat{n}(\theta,\phi+\omega_c t)\ . \tag{23}$$

$\hat{n}(\theta,\phi)=(\sin\theta\cos\phi,\sin\theta\sin\phi,\cos\theta)$ is a unit vector in the direction (θ,ϕ). Substituting into (22) and setting $\vec{v}(\vec{k})=\hbar\vec{k}/m$ for free electrons yields an exact formula for the magnetoconductivity,

$$\sigma_{\alpha\beta}=\frac{ne^2}{m\omega_c}\frac{3}{4\pi}\int d\Omega\, n_\beta(\theta,\phi)\int_0^\infty d\phi' n_\alpha(\theta,\phi+\phi')\times P(\theta,\phi;\phi')\ , \tag{24}$$

where $P(\theta,\phi;\phi')$ is the survival probability for rotation by an angle ϕ',

$$P(\theta,\phi;\phi')=\exp\left[-\int_0^{\phi'}\frac{d\phi''}{\omega_c\tau(\theta,\phi+\phi'')}\right]\ . \tag{25}$$

Breaking the range of integration of ϕ' into sections of length 2π and using the periodicity of $\hat{n}(\theta,\phi)$ and $\tau(\theta,\phi)$ leads to a (summable) geometric series. The formula for $\sigma_{\alpha\beta}$ reduces to

$$\sigma_{\alpha\beta}=\frac{ne^2}{m\omega_c}\frac{3}{4\pi}\int d\Omega\, n_\beta(\theta,\phi)[1-P(\theta)]^{-1}\times\int_0^{2\pi}d\phi' n_\alpha(\theta,\phi+\phi')P(\theta,\phi;\phi') \tag{26}$$

with $P(\theta)\equiv P(\theta,\phi;2\pi)$ being the survival probability for a complete revolution.

For $\vec{Q}=Q\hat{x}$, σ_{xz}, σ_{zx}, σ_{yz}, and σ_{zy} all vanish by symmetry.[17] In the high-field limit, the exponential in (25) can be expanded in powers of $1/H$, yielding an expansion of (26). Using the symmetry of $\tau(\theta,\phi)$, it can be shown that the leading terms are

$$\begin{aligned}
\sigma_{xx}&\cong\frac{ne^2}{m\omega_c^2}\left\langle\frac{1}{\tau}\right\rangle_\perp\ ,\\
\sigma_{xy}&=-\sigma_{yx}\cong-\frac{ne^2}{m\omega_c}\ ,\\
\sigma_{yy}&\cong\frac{ne^2}{m\omega_c^2}\left\langle\frac{1}{\tau}\right\rangle_{||}\ ,\\
\sigma_{zz}&\cong\frac{ne^2}{m}\frac{3}{4\pi}\int d\Omega\cos^2\theta\left[\frac{1}{2\pi}\int_0^{2\pi}\frac{d\phi'}{\tau(\theta,\phi')}\right]^{-1}\ ,
\end{aligned} \tag{27}$$

the parallel and perpendicular averages having the same definitions as before.

The resistivity and Hall coefficient are obtained by inverting the magnetoconductivity. From (27), the saturation values of the transverse resistivities are

$$\rho_\perp^{(t)}\to\frac{m}{ne^2}\left\langle\frac{1}{\tau}\right\rangle_\perp\ ,\quad \rho_{||}^{(t)}\to\frac{m}{ne^2}\left\langle\frac{1}{\tau}\right\rangle_{||}\ ,\quad \omega_c\tau>1 \tag{28}$$

equal to the resistivities $\rho_\perp'$ and $\rho_{||}'$, computed with a rigidly shifted distribution function. For $\omega_c\tau>1$, the Hall coefficient has the free-electron value $R_0=-1/(nec)$.

The three resistivities ($\rho_{||}^{(t)}$, $\rho_{\perp,2}^{(t)}$, and $\rho_\perp^{(l)}$) and the Hall coefficient ($R_\perp$), evaluated from (26) for $\tau(\theta)$ given by (1), are plotted in Figs. 8, 9, and 10. The low-field magnetoresistance "knees," which have been observed in potassium,[18] are linear in B, all the way to $B=0$.

For $\omega_c\tau>1$, the transverse resistivities (both for $\vec{Q}||\vec{B}$ and $\vec{Q}\perp\vec{B}$) are equal to the resistivities computed with a rigidly shifted distribution function. For a spherical Fermi surface, this can be proven even without making a relaxation-time approximation.[19]

V. INDUCED TORQUE

In an induced-torque experiment (Fig. 11), a single-crystal sphere is suspended in a uniform magnetic field $\vec{B}$.

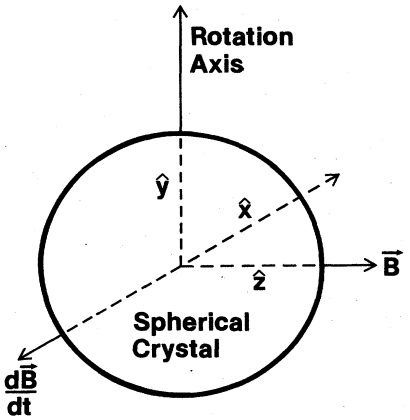

FIG. 11. Induced-torque experiment. Rotation of $\vec{B}$ induces currents, which interact with $\vec{B}$, producing a torque about the suspension axis.

Slow rotation of $\vec{B}$ (or the crystal) induces circulating currents, giving rise to a torque on the sample. The torque magnitude depends on the induced current, which in turn depends on the magnetoconductivity of the sample in the field $\vec{B}$.

An exact theory of the induced torque, depending only on Faraday's law of induction, has been derived for a general magnetoconductivity tensor.[20] If there is no longitudinal-transverse mixing, i.e., σ_{xz}, σ_{zx}, σ_{yz}, and σ_{zy} all vanish, the formula for the torque N about the rotation axis reduces to

$$N \propto \frac{\rho_{xx}+\rho_{zz}}{(\rho_{xx}+\rho_{zz})(\rho_{yy}+\rho_{zz})-\rho_{xy}\rho_{yx}} . \tag{29}$$

The proportionality constant, which is $4\pi a^5\omega B^2/15c^2$, depends on the sphere radius a and rotation frequency ω. At low fields, when the induced currents circulate in the y-z plane normal to $d\vec{B}/dt$, the Hall resistivity is negligible, yielding

$$N \propto \frac{1}{\rho_{yy}+\rho_{zz}} , \quad \omega_c\tau<1 . \tag{30}$$

At high fields, when the Lorentz force rotates the current loops into the horizontal x-z plane, the Hall resistivity dominates, yielding

$$N \propto \frac{\rho_{xx}+\rho_{zz}}{-\rho_{xy}\rho_{yx}} , \quad \omega_c\tau>1 . \tag{31}$$

The $\vec{Q}$-vector orientation of the experimental samples studied in Refs. 9 and 10 is not known. For simplicity, we suppose $\vec{Q}$ lies in the rotation plane. Then, at the maximum of the twofold torque pattern, $\vec{Q}\perp\vec{B}$; and at the minimum, $\vec{Q}\parallel\vec{B}$. For $\vec{Q}\perp\vec{B}$, $\rho_{yy}=\rho_{\perp,2}^{(t)}$ and $\rho_{zz}=\rho_{\perp}^{(l)}$; for $\vec{Q}\parallel\vec{B}$, $\rho_{yy}=\rho_{\perp,1}^{(t)}$ and $\rho_{zz}=\rho_{\parallel}^{(l)}$. The low-field torque anisotropy $\mathscr{R}\equiv N_{\max}/N_{\min}$ is thus

$$\mathscr{R}\cong\frac{\rho_{\perp,1}^{(t)}+\rho_{\parallel}^{(l)}}{\rho_{\perp,2}^{(t)}+\rho_{\perp}^{(l)}} , \quad \omega_c\tau<1 . \tag{32}$$

As $B\to 0$, the perpendicular and parallel magnetoresistivities are equal, respectively, to the zero-field resistivities $\rho_\perp$ and $\rho_\parallel$. The zero-field limit of the torque anisotropy is thus

$$\mathscr{R}_0=\frac{\rho_\perp+\rho_\parallel}{2\rho_\perp}=\frac{1+\gamma}{2} , \tag{33}$$

as deduced previously.[4] γ is the zero-field resistivity anisotropy. For the model (1) with $\eta=25°$ and $\tau'=0.05$, $\gamma=1.30$, so that $\mathscr{R}_0=1.15$.

Since the induced-current loops rotate into the horizontal plane as B increases, it might be expected that the torque would be isotropic at high fields. For $\vec{Q}\perp\vec{B}$, $\rho_{xx}=\rho_{\parallel}^{(t)}$, $\rho_{zz}=\rho_{\perp}^{(l)}$, and $\rho_{yx}=-\rho_{xy}=R_\perp B$; for $\vec{Q}\parallel\vec{B}$, $\rho_{xx}=\rho_{\perp,1}^{(t)}$, $\rho_{zz}=\rho_{\parallel}^{(l)}$, and $\rho_{yx}=-\rho_{xy}=R_\parallel B$. The high-field torque anisotropy is thus

$$\mathscr{R}\cong\left[\frac{R_\parallel}{R_\perp}\right]^2\frac{\rho_{\parallel}^{(t)}+\rho_{\perp}^{(l)}}{\rho_{\perp,1}^{(t)}+\rho_{\parallel}^{(l)}} , \quad \omega_c\tau>1 . \tag{34}$$

For an anisotropic relaxation-time model, the high-field Hall coefficient is isotropic. (In potassium, the high-field Hall-coefficient anisotropy $R_\parallel/R_\perp$ is typically about 1.1, although it can be as large as 1.3.[5]) Setting $R_\parallel/R_\perp=1$ yields

$$\mathscr{R}\cong\frac{\rho_{\parallel}^{(t)}+\rho_{\perp}^{(l)}}{\rho_{\perp,1}^{(t)}+\rho_{\parallel}^{(l)}} , \quad \omega_c\tau>1 . \tag{35}$$

If the magnetoresistance were independent of field orientation, i.e., $\rho_{\parallel}^{(t)}=\rho_{\parallel}^{(l)}$ and $\rho_{\perp}^{(t)}=\rho_{\perp}^{(l)}$, the high-field torque ratio $\mathscr{R}$ would indeed be unity, implying a decrease compared to its zero-field value.

The magnetoresistance, however, depends on the field direction. This is illustrated for the model (1) in Figs. 8 and 9. For small η, the perpendicular resistivities are only slightly affected by the magnetic field, all being approximately equal. But the high-field, parallel resistivity is much larger for $\vec{B}\perp\vec{Q}$ than for $\vec{B}\parallel\vec{Q}$, thus causing the torque anisotropy to increase.

In high fields, the transverse resistivities $\rho_{\parallel}^{(t)}$ and $\rho_{\perp}^{(t)}$ are equal to $\rho'_\parallel$ and $\rho'_\perp$, the resistivities computed with a rigidly shifted distribution function; the longitudinal resistivity $\rho_{\parallel}^{(l)}$, being field independent, is equal to the zero-field resistivity $\rho_\parallel$. The high-field limit of the torque anisotropy (35) is thus

$$\mathscr{R}_\infty=\frac{\delta+\gamma'}{1+\epsilon\gamma} , \tag{36}$$

where $\gamma'\equiv\rho'_\parallel/\rho'_\perp$, $\delta\equiv\rho_{\perp}^{(l)}/\rho_{\perp}^{(t)}$, and $\epsilon\equiv\rho_\perp/\rho'_\perp$. For the model (1) with $\eta=25°$ and $\tau'/\tau=0.05$, $\delta=0.85$, $\epsilon=0.81$, $\gamma=1.30$, and $\gamma'=4.71$, so that $\mathscr{R}_\infty=2.70$.

The torque ratio, evaluated from (29) for the model (1), is plotted in Fig. 12.[21] The small dip at low fields is a consequence of the torque formula, the resistivities themselves increasing monotonically. The initial decrease, which may be masked in a polydomain sample, arises from the linear field dependence of the ($\vec{Q}\perp\vec{B}$) resistivities in the denominator of the torque-ratio formula (32).

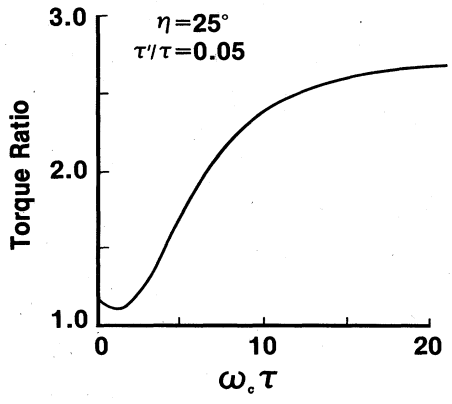

FIG. 12. Theoretical ratio of the torque maximum and minimum. The zero-field and high-field values are $\mathscr{R}_0=1.15$ and $\mathscr{R}_\infty=2.70$.

VI. DISCUSSION

The low-field, induced-torque experiments by Elliott and Datars[9,10] show that the residual-resistivity anisotropy of sodium and potassium increases with increasing magnetic field. For potassium, the zero-field torque anisotropy (for the samples studied) was in the range 1.05—1.25. In an applied magnetic field, this anisotropy increased by about an order of magnitude.

If one believes that potassium and sodium have cubic symmetry, these results are triply perplexing. First, how can the zero-field resistivity be anisotropic? Second, how can the resistivity anisotropy increase in a magnetic field? Third, how can the measured resistivity anisotropy vary for nominally identical samples?

The zero-field resistivity anisotropy is explained by anisotropic scattering, caused by the charge-density-wave potential.[4] As we have shown here, this same mechanism also explains the increase of the resistivity anisotropy in a magnetic field. The uncontrolled domain structure, depending on metallurgical history, explains the variability of the data from sample to sample.

Exact numerical calculations of the zero-field resistivity anisotropy in potassium, based on a microscopic theory of electron-impurity scattering for a charge-density-wave state, yield an anisotropy of about 2.[22] (This value, which applies to a single $\vec{Q}$ domain, is an upper bound for experiment.) By Eq. (33), the zero-field torque anisotropy is about 1.5, agreeing with experiment.

The low-field, induced torque of sodium and potassium spheres is expected to be isotropic if the Fermi surface is spherical. Three symmetry-breaking mechanisms have been suggested: (i) nonspherical samples;[23] (ii) oriented, nonspherical scattering centers; (iii) a nonspherical Fermi surface. The first two have been ruled out.[4,10,24] Only the third, caused by a charge-density-wave structure, explains the main features of the data.

ACKNOWLEDGMENTS

It is a pleasure to thank Xiadong Zhu for helpful discussions. We are grateful to the National Science Foundation and the NSF Materials Research Laboratories Program for financial support.

APPENDIX

The angle η in the relaxation-time model (1) can be estimated if the region of umklapp scattering is determined by the wave-function mixing (rather than by the Fourier components of the impurity potential). The CDW potential $V=G\cos(\vec{Q}\cdot\vec{r})$ mixes the plane-wave state $\vec{k}$ with $\vec{k}\pm\vec{Q}$. The degree of mixing, which is complete (100%) at an energy-gap plane, decreases with increasing distance of the state $\vec{k}$ from the energy gap plane. This continuous change is modeled in (1) by an abrupt transition. The boundary between complete and zero mixing is found by equating the average mixing of the occupied states for the relaxation-time model and a CDW state.

In a CDW state, the electron wave functions satisfy the Schrödinger equation

$$\frac{-\hbar^2}{2m}\nabla^2\psi_{\vec{k}}+G\cos(\vec{Q}\cdot\vec{r})\psi_{\vec{k}}=E_{\vec{k}}\psi_{\vec{k}}\ . \tag{A1}$$

For $\vec{Q}=Q\hat{z}$, the energy denominator for the mixing of the plane-wave state $\vec{k}$ with $\vec{k}\pm\vec{Q}$ is

$$\epsilon_{\vec{k}\pm\vec{Q}}-\epsilon_{\vec{k}}=(\hbar^2/2m)(\pm 2k_zQ+Q^2)\ . \tag{A2}$$

Thus, if $k_z<0$, the state $\vec{k}$ is mixed most with $\vec{k}+\vec{Q}$; if $k_z>0$, the state $\vec{k}$ is mixed most with $\vec{k}-\vec{Q}$.

Because Q is slightly greater than the diameter $2k_F$ of the free-electron Fermi sphere, only the states below the energy gap (at $k_z=\pm Q/2$) are occupied. For these states, an approximate solution is derived as follows.[4] For $k_z<0$, we assume that the plane-wave state $\vec{k}$ mixes only with $\vec{k}+\vec{Q}$. This leads to the secular equation

$$\begin{vmatrix} \epsilon_{\vec{k}}-E_{\vec{k}} & \frac{1}{2}G \\ \frac{1}{2}G & \epsilon_{\vec{k}+\vec{Q}}-E_{\vec{k}} \end{vmatrix}=0\ , \tag{A3}$$

which has two solutions for the energy eigenvalue $E_{\vec{k}}$. The lower one, belonging to the state below the gap, is

$$E_{\vec{k}}=\tfrac{1}{2}(\epsilon_{\vec{k}}+\epsilon_{\vec{k}+\vec{Q}})-\tfrac{1}{2}[(\epsilon_{\vec{k}+\vec{Q}}-\epsilon_{\vec{k}})^2+G^2]^{1/2},\quad k_z<0\ . \tag{A4}$$

If the corresponding eigenfunction is denoted by

$$\psi_{\vec{k}}=\cos(\xi)e^{i\vec{k}\cdot\vec{r}}-\sin(\xi)e^{i(\vec{k}+\vec{Q})\cdot\vec{r}}\ , \tag{A5}$$

the degree of mixing $\zeta(\vec{k})\equiv 2\sin^2\xi$ is

$$\zeta(\vec{k})=2(\epsilon_{\vec{k}}-E_{\vec{k}})^2/[(\tfrac{1}{2}G)^2+(\epsilon_{\vec{k}}-E_{\vec{k}})^2]\ . \tag{A6}$$

For $k_z>0$, we assume that the plane-wave state $\vec{k}$ mixes only with $\vec{k}-\vec{Q}$, yielding the energy eigenvalue

$$E_{\vec{k}}=\tfrac{1}{2}(\epsilon_{\vec{k}}+\epsilon_{\vec{k}-\vec{Q}})-\tfrac{1}{2}[(\epsilon_{\vec{k}-\vec{Q}}-\epsilon_{\vec{k}})^2+G^2]^{1/2},\quad k_z>0\ . \tag{A7}$$

The degree of mixing $\zeta(\vec{k})$ is the same as for $k_z<0$.

It is convenient to introduce the dimensionless variables $u=k_x/Q$, $v=k_y/Q$, $\kappa=(u^2+v^2)^{1/2}$, and

$$w=\begin{cases}(k_z+\frac{1}{2}Q)/Q, & k_z<0\\ (k_z-\frac{1}{2}Q)/Q, & k_z>0\end{cases}\ . \tag{A8}$$

Making these substitutions yields

$$E_{\vec{k}}=\frac{\hbar^2Q^2}{2m}[\kappa^2+w^2+\tfrac{1}{4}-(w^2+\alpha^2)^{1/2}]\ , \tag{A9}$$

$$\zeta(\vec{k})=1-w(w^2+\alpha^2)^{-1/2}\ , \tag{A10}$$

with $\alpha\equiv mG/(\hbar^2Q^2)$.

We assume that the Fermi surface makes critical contact with the energy-gap planes, as shown in Fig. 2. For $\vec{k}=\frac{1}{2}\vec{Q}$, $\epsilon_{\vec{k}}=\epsilon_{\vec{k}-\vec{Q}}=\hbar^2(\frac{1}{2}Q)^2/2m$. Substituting in (A7) yields the Fermi energy

$$E_F=\hbar^2(\tfrac{1}{2}Q)^2/2m-\tfrac{1}{2}G\ . \tag{A11}$$

From (A9), the equation of the Fermi surface is then

$$\kappa^2=(w^2+\alpha^2)^{1/2}-w^2-\alpha\ . \tag{A12}$$

The magnitude of Q as a function of G is found by equating the volume within the Fermi surface (A12) to the volume $(4\pi/3)k_F^3$ of the free-electron Fermi sphere, yielding

$$k_F^3=\tfrac{3}{4}Q^3\left[\tfrac{1}{2}(\tfrac{1}{4}+\alpha^2)^{1/2}+\alpha^2\sinh^{-1}\left[\frac{1}{2\alpha}\right]-\tfrac{1}{12}-\alpha\right] \tag{A13}$$

with $\alpha=mG/(\hbar^2Q^2)$ and $k_F^3=3\pi^2n$. Finally, averaging the mixing (A10) over the occupied states, we obtain

$$\langle\zeta\rangle=1-\tfrac{3}{2}(Q/k_F)^3[\tfrac{1}{8}-(\tfrac{1}{12}+\alpha-\tfrac{2}{3}\alpha^2)(\tfrac{1}{4}+\alpha^2)^{1/2}+(1-\tfrac{2}{3}\alpha)\alpha^2]\ . \tag{A14}$$

In the relaxation-time model, the degree of mixing $\zeta=0$ for $|k_z|<k_F\cos\eta$ and $\zeta=1$ for $k_F\cos\eta<|k_z|<k_F$. The average mixing of the occupied states is then

$$\langle\zeta\rangle=1-\tfrac{3}{2}\cos\eta+\tfrac{1}{2}\cos^3\eta\ . \tag{A15}$$

For sodium, the free-electron Fermi energy $E_F^0=\hbar^2k_F^2/2m$ is 3.24 eV; the CDW-potential amplitude G, equal to the threshold energy of the optical absorption anomaly, is 1.2 eV; and $G/E_F^0=0.37$.[25] For potassium, $E_F^0=2.12$eV, $G=0.6$eV, and $G/E_F^0=0.28$.[26,27] Solving numerically Eqs. (A13), (A14), and (A15) yields $\eta=27°$ for sodium and $\eta=24°$ for potassium.

[1]For an experimental and theoretical review of charge-density waves in simple metals, see A. W. Overhauser, Adv. Phys. **27**, 343 (1978).

[2]J. A. Schaefer and J. A. Marcus, Phys. Rev. Lett. **27**, 935 (1971).

[3]F. W. Holroyd and W. R. Datars, Can. J. Phys. **53**, 2517 (1975).

[4]M. F. Bishop and A. W. Overhauser, Phys. Rev. B **18**, 2477 (1978).

[5]X. Zhu and A. W. Overhauser, Phys. Rev. B **30**, 622 (1984).

[6]P. G. Coulter and W. R. Datars, Phys. Rev. Lett. **45**, 1021 (1980).

[7]P. G. Coulter and W. R. Datars, Solid State Commun. **43**, 715 (1982).

[8]M. Huberman and A. W. Overhauser, Phys. Rev. B **25**, 2211 (1982).

[9]M. Elliott and W. R. Datars, Solid State Commun. **46**, 67 (1983).

[10]M. Elliott and W. R. Datars, J. Phys. F **13**, 1483 (1983).

[11]I. M. Lifshitz, M. Ya. Azbel, and M. I. Kaganov, Zh. Eksp. Teor. Fiz. **31**, 63 (1956) [Sov. Phys.—JETP 4, 41 (1957)].

[12]B. Llewellyn, D. McK. Paul, D. L. Randles, and M. Springford, J. Phys. F **7**, 2531 (1977).

[13]A. H. Wilson, *Theory of Metals,* 2nd edition (Cambridge University Press, Cambridge, England, 1953); N. W. Ashcroft and N. D. Mermin, *Solid State Physics* (Holt, Rinehart and Winston, New York, 1976).

[14]It is perhaps surprising that the transverse resistance is field dependent, even though the cyclotron motion does not change an electron's relaxation time. The same effect occurs in the two-band model. See J. M. Ziman, *Principles of the Theory of Solids* (Cambridge University Press, Cambridge, England, 1964).

[15]A. B. Pippard, Proc. R. Soc. London **A282**, 464 (1964).

[16]F. Reif, *Fundamentals of Statistical and Thermal Physics* (McGraw-Hill, New York, 1965); N. W. Ashcroft and N. D. Mermin, *Solid State Physics* (Holt, Rinehart and Winston, New York, 1976).

[17]If $\vec{E}$ is parallel to $\vec{B}$, so is $\vec{J}$, implying $\sigma_{xz}=\sigma_{yz}=0$. By the Onsager symmetry relations, σ_{zx} and σ_{zy} also vanish.

[18]J. Babiskin and P. G. Siebenmann, Phys. Kondens. Mater. 9, 113 (1969); H. Taub, R. L. Schmidt, B. W. Maxfield, and R. Bowers, Phys. Rev. B **4**, 1134 (1971).

[19]D. K. Wagner, Phys. Rev. B **5**, 336 (1972); and Ph.D. thesis, Cornell University, 1971. If the Fermi surface is not spherical, the steady-state distribution function for $\omega_c\tau>1$ is no longer a rigidly shifted equilibrium distribution. It still, however, depends only on the Fermi-surface geometry and not on the scattering mechanisms.

[20]P. B. Visscher and L. M. Falicov, Phys. Rev. B **2**, 1518 (1970).

[21]In order to compare Fig. 12 with experiment, note that typically $\omega_c\tau\approx5$ at 0.2 T. (The procedure used in Ref. 10 to determine $\omega_c\tau$ may not be valid for an anisotropic relaxation time.)

[22]S. DeGennaro and E. Borchi, J. Phys. F **12**, 963 (1982); **12**, 2363 (1982). We have used the results for $G/E_F=0.3$, the value appropriate to potassium. The uncertainty of the theoretical calculation stems primarily from the unknown impurity potential. We have disregarded the calculations using a screened impurity pseudopotential, since the many-electron dielectric function $\epsilon(q)$ is not well known near $q=2k_F$.

[23]J. S. Lass, Phys. Rev. B **13**, 2247 (1976).

[24]D. Gugan, J. Phys. F **12**, L173 (1982).

[25]B. Hietel and H. Mayer, Z. Phys. **264**, 21 (1973).

[26]H. Mayer and M. H. El Naby, Z. Phys. **174**, 269 (1963).

[27]A. W. Overhauser, Phys. Rev. Lett. **13**, 190 (1964); A. W. Overhauser and N. R. Butler, Phys. Rev. B 14, 3371 (1976).